THERMO-CHEMICAL CONVECTION IN EUROPA'S ICY SHELL WITH SALINITY. L. Han, A.P. Showman, *Department of Planetary Sciences and Lunar and Planetary Laboratory, University of Arizona, Tucson, AZ, 85721, USA (lhan@lpl.arizona.edu).*

Summary: Europa's icy surface displays numerous pits, uplifts, and chaos terrains that have been suggested to result from solid-state thermal convection in the ice shell, perhaps aided by partial melting [1-4]. However, numerical simulations of thermal convection show that plumes have insufficient buoyancy to produce surface deformation [5-6]. Here we present numerical simulations of thermo-chemical convection to test the hypothesis that convection with salinity can produce Europa's pits and domes. Our simulations show that domes (200-300 m) and pits (300-400 m) comparable to the observations can be produced in an ice shell of 15 km thick with 5-10% compositional density variation if the maximum viscosity is less than 10^{18} Pa sec.

Introduction: Europa's surface displays two dominant terrain types, the ridged plains, which consist of multiple generations of overprinted ridge pairs, and the mottled terrains, which are distributed with chaos and numerous small (3–30 km-diameter) pits, uplifts, and irregularly shaped landforms [1,4, 7-9]. It has been suggested that pits, domes, and chaos resulted from thermal convection in the ice shell, perhaps aided by partial melting [1-4]. Showman and Han [5-6] performed numerical simulations of thermal convection, showing that the uplifted topography produced in thermal convection models is far less than the observations.

So far, all the numerical simulations of convection in Europa's ice shell assume a pure-ice composition[10-11,5-6]. However, evidence suggests that salts are present on Europa's surface. Galileo NIMS spectra contain features that are well fit by several hydrated sulfates [12] and solidified, hydrated sulfuric acid [13]. Motivated by the difficulty of explaining domes with thermal convection in pure ice, Pappalardo and Barr [14] suggested that the domes instead result from compositional density contrasts in a salty ice shell.

To date, no numerical simulations of convection in Europa's ice shell have included the effects of salinity. Here we present two-dimensional numerical simulations of thermo-chemical convection in Europa's icy shell to evaluate the effects of salinity on convection patterns, icy shell structure, and surface topography.

Model and Methods. We used the particle-in-cell (PIC) finite element code ellipsis3d [15] to solve the equations governing thermo-chemical convection in Europa's salty ice shell in 2-D cartesian geometry. The velocity boundary conditions are reflective on the sides and free-slip on the top and bottom. The temperature boundary condition at the bottom is fixed (270 K), as required by the underlying ocean, and the top is held at 95 K. For the simulations presented here, the layer thickness is 15 km. In these preliminary simulations, no tidal heating is included.

Temperature-dependent Newtonian viscosity is implemented. The temperature-dependent viscosity is represented as follows:

$$\eta(T) = \min\left[\eta_{\text{cutoff}},\ \eta_0 \exp\left\{A\left(\frac{T_m}{T} - 1\right)\right\}\right] \qquad (1)$$

where T is temperature, T_m is melting temperature, and $\eta_0 \approx 10^{13}$ Pa sec is the viscosity at the melting temperature. We adopt $A = 26$, corresponding to an activation energy of 60 kJ mole^{-1}. The cutoff viscosity, η_{cutoff}, ranges from 10^{17} to 10^{21} Pa sec, implying a viscosity contrast of 10^4–10^8.

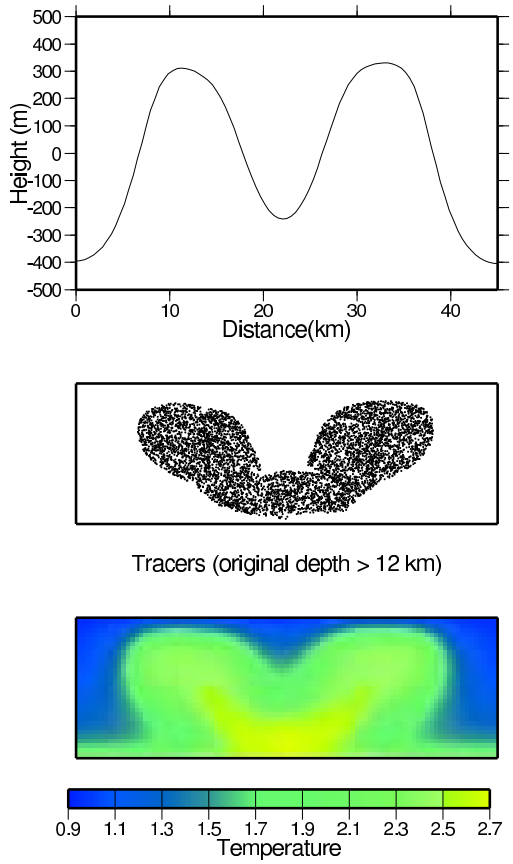

Figure 1: Dynamic topography, composition, and temperature for a simulation in a domain 45 km wide and 15 km deep. In the middle panel, the black material represents the low-density ice that was initially in the bottom 3 km of the domain.

Results. Figure 1 displays the results from a model in a domain 45 km wide and 15 km deep, which is initialized with two different layers. The top layer (from 0–12 km depth) has a density of 1100 kg/m^3, and the bottom layer (from 12–15 km depth) has a density of 1000 kg/m^3. The upper layer represents dense, saline ice, while the low-density material in the bottom 3 km represents low-salinity ice envisioned to result from loss of salts due to partial melting near the base of the ice shell [14]. The cutoff viscosity is 10^{17} Pa sec. The initial temperature increases linearly from the top (95 K) to the bottom (270 K)

with a small initial disturbance. In the simulation, the low-density material develops numerous small-scale (∼few-km-wide) convective instabilities before ascending en masse into a 20 km-wide diapir, which splits in two as dense, salty ice descends through its center (Fig. 1). Uplifts 250–300 m tall and pits about 250–400 m deep, with diameters of about 15 km, are formed. These features result directly from the horizontal buoyancy contrasts; the combined buoyancy from temperature and compositional variations far exceeds the thermal buoyancy alone, which explains the large topography relative to that obtained in the earlier, pure-ice simulations [5-6]. Eventually, the lower density material from the bottom mixes up with the higher density material at the top, and the strong surface topography disappears.

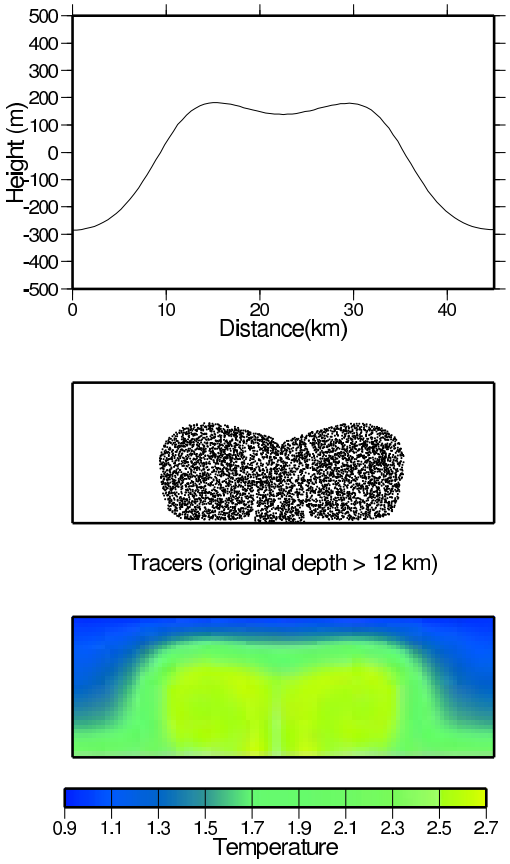

Figure 2: Dynamic topography, composition, and temperature for a simulation in a domain 45 km wide and 15 km deep. In the middle panel, the black material represents the material that was initially in the bottom 3 km of the domain.

Figure 2 gives the results from a model in a domain 45 km wide and 15 km deep. The initial condition is similar to that in Fig. 1 except that the bottom density is only 5% smaller than the top density. However, this simulation includes a simple parameterization for partial melting, and melt drainage, of ice containing low-eutectic-temperature salts. Partial melting is assumed to begin at temperatures of 220 K, leading to a reduction in density of up to 5% as temperatures rise to 250 K or above. Uplifts 200 m in height and pits 300–400 m in depth, with diameters of 20 km, are produced on the the surface. These topographies are comparable to the observed pits and domes on Europa. If the compositional density contrast is increased, then even taller domes and deeper pits can be produced.

Simulations show that the viscosity structure plays a key role in determining whether topography can occur. In a 15-km-thick ice shell with 5–10% compositional density contrasts, the simulations cannot produce the observed pits and domes if the viscosity in the cold region exceeds 10^{19} Pa sec.

Conclusions and Discussions: Thermo-chemical convection in Europa's icy shell can produce pits and domes comparable to the observations under appropriate conditions. If the compositional density variation is 5–10% and the maximum viscosity is less than 10^{18} Pa sec, thermo-chemical convection in a 15 km-thick ice shell produces pits and uplifts with topographic amplitudes of 200–400 m. But our simulations show that convection under the same conditions cannot produce the observed pits and domes if the viscosity in the cold region exceeds 10^{19} Pa sec. Conceivably, brittle behavior in the cold near-surface ice could allow the lithospheric deformation necessary for uplifts and pits to form [6].

Future Work: Elasticity near the surface and tidal heating within the ice shell can strongly affect thermo-chemical convection and its related features on Europa; these will be considered in the future. Although the pits and uplifts in our simulations are transient features, it is possible that melt-filled fractures may continue to inject salt into the ice shell and that partial melting near the base of the shell (perhaps driven by tidal heating) would produce a continuing supply of fresh, low-density ice there. Our future models will include these sources and sinks to determine whether pits and uplifts can be continually generated on Europa.

This work is supported by the NASA PG&G program.

References: **[1].** Pappalardo, R.T., et al. (1998) Nature 391, 365-368. **[2].** Head, J.W. and R.T. Pappalardo (1999) JGR 104, 27143-27155. **[3].** Collins, G.C., et al. (2000) JGR 105, 1709-1716. **[4].** Spaun, N.A. (2002) Ph.D. Thesis, Brown University. **[5].** Showman, A.P. and L. Han (2004a) JGR 109, E01010, doi:10.1029/2003E002103. **[6].** Showman, A.P. and L. Han (2004b) Lunar Planet. Sci. Conf. XXXV, [abstract 1466]. **[7].** Greeley, R., et al. (1998) Icarus 135, 4-24. **[8].** Riley, J., et al. (2000) JGR 105, 22599-22615. **[9].** Greenberg, R., et al. (2003) Icarus 161, 102-126. **[10].** Sotin, C., et al. (2002) GRL 29, 10.1029/2001GL013884. **[11].** Tobie, G., et al. (2003) JGR 108, doi:10.1029/2003JE002099. **[12].** McCord, T.B., et al. (1999) JGR 104(E5), 11,827-11,851. **[13].** Carlson, R.W., et al. (1999) Science 286, 97-99. **[14].** Pappalardo, R.T. and A.C. Barr (2004a) GRL 31, L01701, doi:10.1029/2003GL019202. **[15].** Moresi, L., et al. (2003) J. Comput. Phys. 184, 476-497.